science.sciencemag.org/cgi/content/full/science.abb4557/DC1

Supplementary Materials for

Effective containment explains subexponential growth in recent confirmed COVID-19 cases in China

Benjamin F. Maier,* and Dirk Brockmann

*Corresponding author. Email: bfmaier@physik.hu-berlin.de

Published 8 April 2020 on *Science* First Release
DOI: 10.1126/science.abb4557

This PDF file includes:

Other Supplementary Materials for this manuscript include the following:
(available at science.sciencemag.org/cgi/content/full/science.abb4557/DC1)

MDAR Reproducibility Checklist (.pdf)

Materials and Methods

We rely on case number data provided by the Center for Systems Science and Engineering of Johns Hopkins University who provided up to two updates per day on the number of laboratory-confirmed cases globally until Feb. 12th (*9*). For this time period, the group integrated and curated case data manually collected at four sources: the World Health Organization (WHO), the US Centers for Disease Control and Prevention (CDC), the European Centre for Disease Prevention and Control (ECDC), the Chinese physician's platform DXY.cn, and the National Health Commission of the People's Republic of China (NHC). The published data comprises total confirmed cases, total deaths, and total recovered cases as a function of time for each affected location. We focus on the number of total confirmed cases $C(t)$. On Feb. 12th, the case definition was changed by Chinese authorities which labeled a large number of clinically diagnosed cases as confirmed (as opposed to pure laboratory-confirmed), leading to a discontinuity in the curves. For the fitting procedure in the main text, we therefore only consider data prior to Feb. 12th, 6am UTC. Case numbers following this date correspond to daily updates.

The data is provided as pairs $(t_i, C(t_i))$ of time stamp and respective case number for each province. We omitted case numbers $C(t_i)$ that remained constant between two consecutive time stamps $C(t_i) = C(t_{i-1})$ since we assume these data points have been copied when no updates were available at a certain time. In order to obtain the aggregated data for all provinces except Hubei, time points $\tilde{t}$ were chosen with step size $\Delta\tilde{t} = (1/2)$d. For each province, the case number value $C(\tilde{t})$ was obtained by means of linear interpolation between $C(t_i)$ and $C(t_{i+1})$ for $t_i \leq \tilde{t} < t_{i+1}$. All processed data is available online (*23*).

We obtained the population size N of each of the affected Chinese provinces from the Geonames project (*24*).

Fits were performed using the Levenberg–Marquardt method of least squares after tests with the Nelder–Mead method yielded equal or similar results. We fixed the epidemiological parameters $T_I = 8\,\mathrm{d}$ (duration of infection) and basic reproduction number $R_{0,\mathrm{free}} = \alpha T_I = 6.2$. For each confirmed cases data set, we set the initial conditions $X(t_0) = C(t_0)/N$, $I(t_0) = (I_0/X_0)X(t_0)$, and $S(t_0) = 1 - I(t_0) - X(t_0)$. Since the number of unidentified infectious is unknown per definition, the prefactor $I_0/X_0 \geq 10^{-3}$ was chosen as a fit parameter. The remaining fit parameters were quarantine rate $\kappa > 0$ and containment rate $\kappa_0 > 0$. For the fit procedure, Eqs. (1)-(4) were integrated using the Dormand–Prince method which implements a fourth-order Runge–Kutta method with step-size control, yielding $I(t)$ and $X(t)$ for every parameter configuration and every data set. The residuals were computed as $\mathcal{R}(t_i) = NX(t_i) - C(t_i)$.

We find that the model accurately reproduces both, the sub-exponential growth as well as the saturating behavior observed in the data discussed in the main text, with the obtained fit parameters compiled in table S1. We find that generally, lower values of the containment rate correlate with higher quarantine rates. This suggests that stronger quarantine implementation requires less public isolation. Yet,broad regions of the parameter space generate similar shapes of growth curves, implying that the exact numerical values of the fit parameters are of less importance than the implications of the mechanisms they comprise.

As the population size was fixed to be equal to the total population of the respective provinces, one might also ask how system size changes the results—for instance, if the outbreak is contained in a small region of a province, the effective population available to the transmission process will be substantially smaller. Therefore, we repeated the fit procedure with N as a free fit parameter to find that the form of $X(t)$ is not altered substantially for different values of N. $I(t)$ can vary more strongly, reflected by a larger variation in I_0. This result suggests that the estimation of the number of infecteds is associated with a larger uncertainty. The general shape of $I(t)$, however, remains

stable such that the inference of the peak time of unidentified infecteds is sound. Furthermore, the model favors larger values of the containment rate κ_0 for larger population sizes in order to reproduce empirical data. This is reasonable because the number of available transmission pathways grows quadratically with the population size, making it easier for the disease to spread faster. In order to still observe sub-exponential growth, a large part of the susceptible population has to be removed quickly. Consistently, we find that a decay of susceptibles is necessary to obtain the observed growth behavior (i.e. $\kappa_0 > 0$). In contrast, one may assume that the containment rate is $\kappa_0 = 0$ if one concurrently assumes that implementation of containment measures was very fast, such that only a very small effective population $N_{\text{eff}} \ll N$ was at risk to obtain the infection, as desrcibend in the Supplementary Text.

Concerning variation in the fixed epidemiological parameters, values in the range of $3 \leq R_{0,\text{free}} \leq 12$ yield results similar to the ones described above when adjusting the infectious period T_I to smaller values for smaller reproduction numbers and larger values for larger reproduction numbers, suggesting that a certain range of transmission rates around $\alpha = 0.6/\text{d}$ to $\alpha = 0.8/\text{d}$ has to be assumed to reproduce the observed growth consistently. Explicitly, the fit results are reasonably robust against variations of the duration of infection in a range of $2.6\,\text{d} \leq T_I \leq 20\,\text{d}$ with concurrent adjustment of $R_{0,\text{free}}$. The analysis does therefore not permit the inference of specific epidemiological parameters.

The analysis material is available online (*23*).

Supplementary Text

Fit Parameters for Main Analysis

In order to facilitate the comparison of quarantine and containment rate between provinces and to the recovery rate, we introduce *public containment leverage*

$$P = \kappa_0/(\kappa_0 + \kappa)$$

that reflects how strong isolation measures affect the general public in comparison to quarantine measures imposed on symptomatic infecteds alone. We further define

$$Q = (\kappa_0 + \kappa)/(\beta + \kappa_0 + \kappa)$$

as the *quarantine probability*, i.e. the probability that an infected was identified and quarantined either in specialized hospital wards or at home. The fit parameters are shown in table S1.

Data for all Affected Provinces

In the following, we analyze how several variants of the model discussed in the main text reflect the growth in case number data $C(t)$ for all 29 affected provinces. In contrast to the data in the main text, we use daily aggregated case numbers that were provided in the same repository by the Center for Systems Science and Engineering of Johns Hopkins University (*9*). The reasoning behind this change is that we aim to model the complete case number growth up to Feb. 20th in the following—in contrast to the main text, where twice-daily case number updates for dates until Feb. 12th were used for the fit procedure and daily updates after Feb. 12th were used for confirmation of the model prediction. Since data after Feb. 12th is only available in a daily aggregated format, we prefer to use daily aggregated data for dates before Feb. 12th, as well, to ensure consistency for the fit procedures. Due to the discussed discontinuity in case data for Hubei, we omit case numbers after Feb. 12th.

Fits for Complete Model

We obtained model parameters following the fitting procedure described in the Material and Methods. We show the resulting model predictions on a log-log scale in fig. S1 to illustrate the successful reproduction of the observed scaling laws. The same results are displayed on a double-linear scale in fig. S2 to show that the later behavior of case number growth is mostly consistent with the empirical observation, as well. The fit parameters are shown in table S2.

Modeling Pure-Quarantine Processes

In order to test the hypothesis that public containment measures are responsible for the observed scaling laws in the growth of case numbers, we investigated a model variant in which only the infected population is targeted by quarantine measures such that the quarantine rate is $\kappa > 0$ and the public containment rate is fixed as $\kappa_0 = 0$. As expected, we find that the case numbers grow exponentially initially for the population sizes given in table S2. In order to obtain reasonable fits from this limiting case of the original model, we have to assume that the implementation of containment strategies was so effective that only a limited effective population $N_{\text{eff}} \ll N$ takes part in the transmission process, which we assume to be an additional fit parameter here. All fits of this model are shown in fig. S3 and fig. S4. We show the respective parameters in table S3. Note that this limiting case cannot account for the growth in Hubei (respective panels a.i), where an unreasonably large number of unidentified infecteds is found.

For this model variant with a comparably low population size for all provinces but Hubei, the exponential depletion of susceptibles through the transmission process is sufficiently severe that immediately, the number of cases can follow a sub-exponential growth. In other words, the strong exponential decay of susceptibles is responsible for the observed scaling laws as in the complete model.

Modeling Pure Containment Processes

We further studied a model variant in which infecteds and susceptibles are isolated by the same mechanisms such that the quarantine rate is fixed as $\kappa = 0$ and the public containment rate is $\kappa_0 > 0$. All fits of this model are shown in fig. S5 and fig. S6. We list the respective parameters in tab. S4. This limiting case explains several growth curves well, e.g. the growth in Hubei (respective panels a.i). Other provinces, where successful quarantine procedures may have played a larger role, are not captured by the model (e.g. Tianjin, panel e.iv, Inner Mongolia, panel f.iv).

Analytical Approximations

In the following, we derive an approximate relationship between the model parameters and the exponent μ of the observed scaling laws t^μ. We assume that containment measures are strong enough such that the depletion of susceptibles is dominated by containment rather than the transmission process (i.e. $I \ll S$ initially). Then, Eq. (1) is effectively linearized with solution

$$S(t) = \exp(-\kappa_0 t).$$

Using this functional form of susceptible depletion in Eq. (2), we obtain an inhomogeneous linear ODE with solution

$$I(t) = I_0 \exp[\zeta(t)]$$
$$\zeta(t) = \frac{\alpha}{\kappa_0}\left(1 - \mathrm{e}^{-\kappa_0 t}\right) - (\beta + \kappa + \kappa_0)t.$$

Because the exponential function is monotonic, the amount of unidentified infecteds $I(t)$ reaches a maximum when $\zeta(t)$ is maximal, i.e. for

$$\partial_t \left[\frac{\alpha}{\kappa_0}\left(1 - \mathrm{e}^{-\kappa_0 t}\right) - (\beta + \kappa + \kappa_0)t\right] = 0$$

which evaluates to

$$t_{\max} = \frac{1}{\kappa_0}\log R_{0,\mathrm{eff}}.$$

At this time, the number of quarantined individuals $X(t)$ will begin to deviate from its initial growth behavior to assume saturation. In order to analyze the growth behavior of confirmed cases during the transient phase between onset and maximum, we analyze the epidemiological curves at a point where half the time has passed until the maximum is reached $t_H = t_{\max}/2$. We approximate $I(t)$ by expanding $\zeta(t)$ around t_H up to second order to obtain

$$\zeta(t) \approx \zeta_0 + \frac{\left(2\alpha + \alpha\log(R_{0,\mathrm{eff}}) - 2\sqrt{R_{0,\mathrm{eff}}}(\beta + \kappa + \kappa_0)\right)}{2\sqrt{R_{0,\mathrm{eff}}}}t - \frac{\alpha\kappa_0}{2\sqrt{R_{0,\mathrm{eff}}}}t^2.$$

Using this approximation, we rewrite the growth of unidentified infecteds as

$$\tilde{I}(t) = \tilde{I}_0 \exp\left[t\left(\frac{\alpha}{\sqrt{R_{0,\mathrm{eff}}}}\left[1 + \frac{1}{2}\log(R_{0,\mathrm{eff}})\right] - (\beta + \kappa + \kappa_0)\right) - \frac{\alpha\kappa_0 t^2}{2\sqrt{R_{0,\mathrm{eff}}}}\right],$$

using a tilde $\tilde{I}$ to highlight that the approximate form of $\zeta(t)$ was used. Hence, our model implies that following gradual containment, the exponential growth of an unconstrained epidemic is suppressed by a Gaussian decay in a second-order approximation which is responsible for the stifled growth. The approximate growth of quarantined individuals follows from Eq. (4) as

$$\begin{aligned}
\tilde{X}(t) &= (\kappa + \kappa_0)\int_0^t dt' \tilde{I}(t') \\
&= \sqrt{\frac{\pi}{2}}\frac{\kappa + \kappa_0}{\sqrt{\alpha\kappa_0}}\tilde{I}_0 R_{0,\mathrm{eff}}^{-\frac{2\beta + 2\kappa + \kappa_0 - \frac{2\alpha}{\sqrt{R_{0,\mathrm{eff}}}}}{4\kappa_0}} \exp\left(\frac{\alpha^2\log^2(R_{0,\mathrm{eff}}) + 4\left(\alpha - \sqrt{R_{0,\mathrm{eff}}}(\beta + \kappa + \kappa_0)\right)^2}{8\alpha\kappa_0\sqrt{R_{0,\mathrm{eff}}}}\right)\times \\
&\quad \times\left[\mathrm{erf}\left(\frac{-\alpha\log(R_{0,\mathrm{eff}}) + 2\sqrt{R_{0,\mathrm{eff}}}(\beta + \kappa + \kappa_0) + 2\alpha(\kappa_0 t - 1)}{2\sqrt{2}\sqrt{\alpha}\sqrt{\kappa_0}\sqrt[4]{R_{0,\mathrm{eff}}}}\right)\right. \\
&\quad \left. - \mathrm{erf}\left(\frac{-2\alpha + \alpha(-\log(R_{0,\mathrm{eff}})) + 2\sqrt{R_{0,\mathrm{eff}}}(\beta + \kappa + \kappa_0)}{2\sqrt{2}\sqrt{\alpha}\sqrt{\kappa_0}\sqrt[4]{R_{0,\mathrm{eff}}}}\right)\right].
\end{aligned}$$

Now, the assumption that the growth of quarantined individuals follows a scaling law in the transient phase as $\tilde{X}(t) = At^{\mu}$ implies that $\log \tilde{X}(t) = \log A + \mu \log t$. Hence, we can compute μ as

$$\mu_{\text{approx}} = \left.\frac{\partial \log X}{\partial \log t}\right|_{t=t_H}$$

$$= \frac{\sqrt{\alpha}\log(R_{0,\text{eff}})\exp\left[-\frac{\left(\alpha-\sqrt{R_{0,\text{eff}}}(\beta+\kappa+\kappa_0)\right)^2}{2\alpha\kappa_0\sqrt{R_{0,\text{eff}}}}\right]}{\sqrt{2\pi}\sqrt{\kappa_0}\sqrt[4]{R_{0,\text{eff}}}\left(\text{erf}\left(\frac{\sqrt{R_{0,\text{eff}}}(\beta+\kappa+\kappa_0)-\alpha}{\sqrt{2}\sqrt{\alpha}\sqrt{\kappa_0}\sqrt[4]{R_{0,\text{eff}}}}\right)-\text{erf}\left(\frac{-2\alpha+\alpha(-\log(R_{0,\text{eff}}))+2\sqrt{R_{0,\text{eff}}}(\beta+\kappa+\kappa_0)}{2\sqrt{2}\sqrt{\alpha}\sqrt{\kappa_0}\sqrt[4]{R_{0,\text{eff}}}}\right)\right)}.$$

In table S5, we compare this estimation to the empirical values presented in Fig. 1 of the main text. We find reasonable agreement, considering the highly approximate nature of the derived expression and the fact that the empirical exponents were obtained using fitting procedures, as well.

Fig. S1.

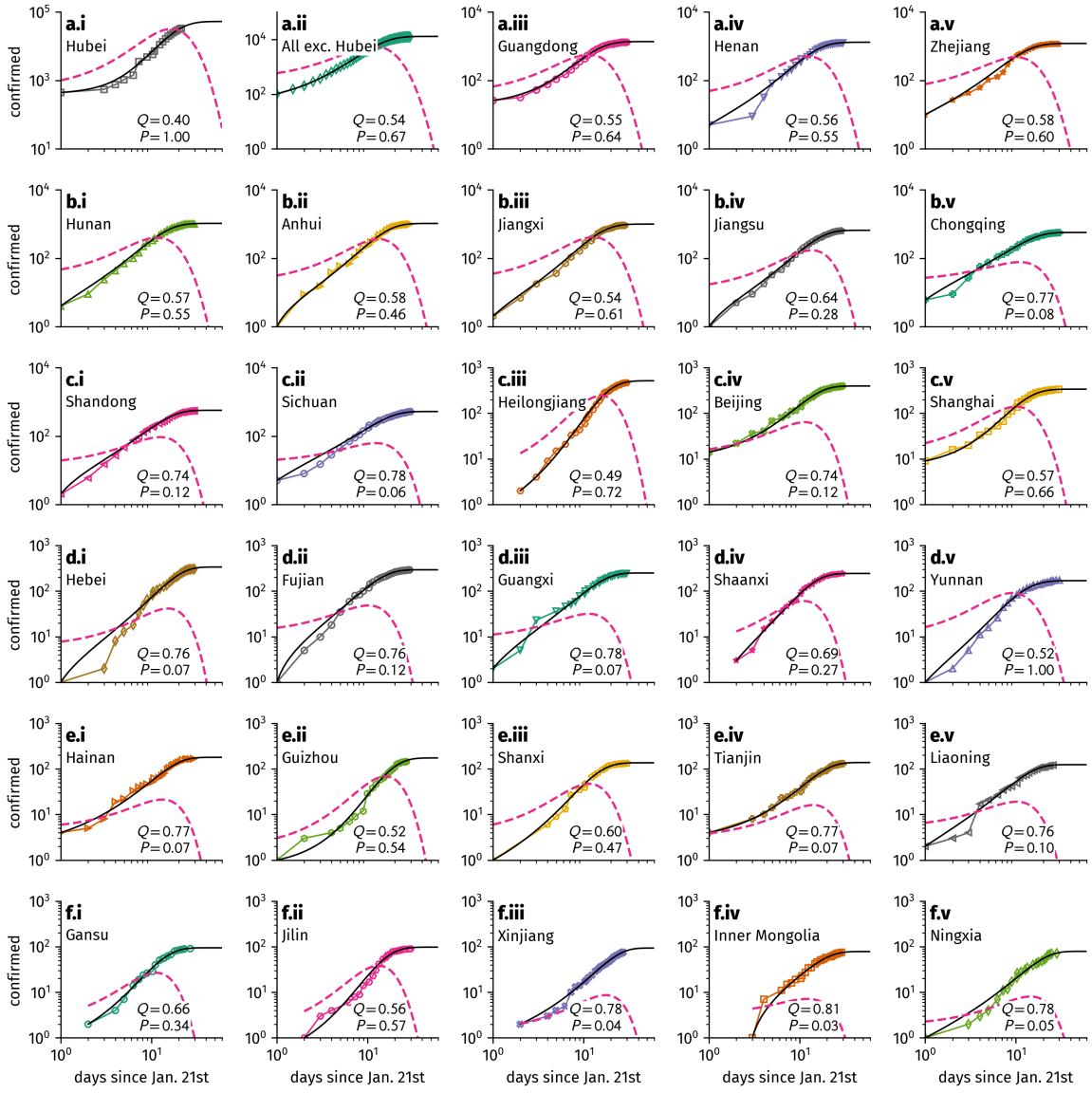

Figure S1: Case numbers of all affected provinces reproduced by the SIR-X model defined by Eqs. (1)-(4) of the main text and the fraction of unidentified infecteds $I(t)$ (dashed line) as obtained from least-squares fits, displayed on a log-log scale.

Fig. S2.

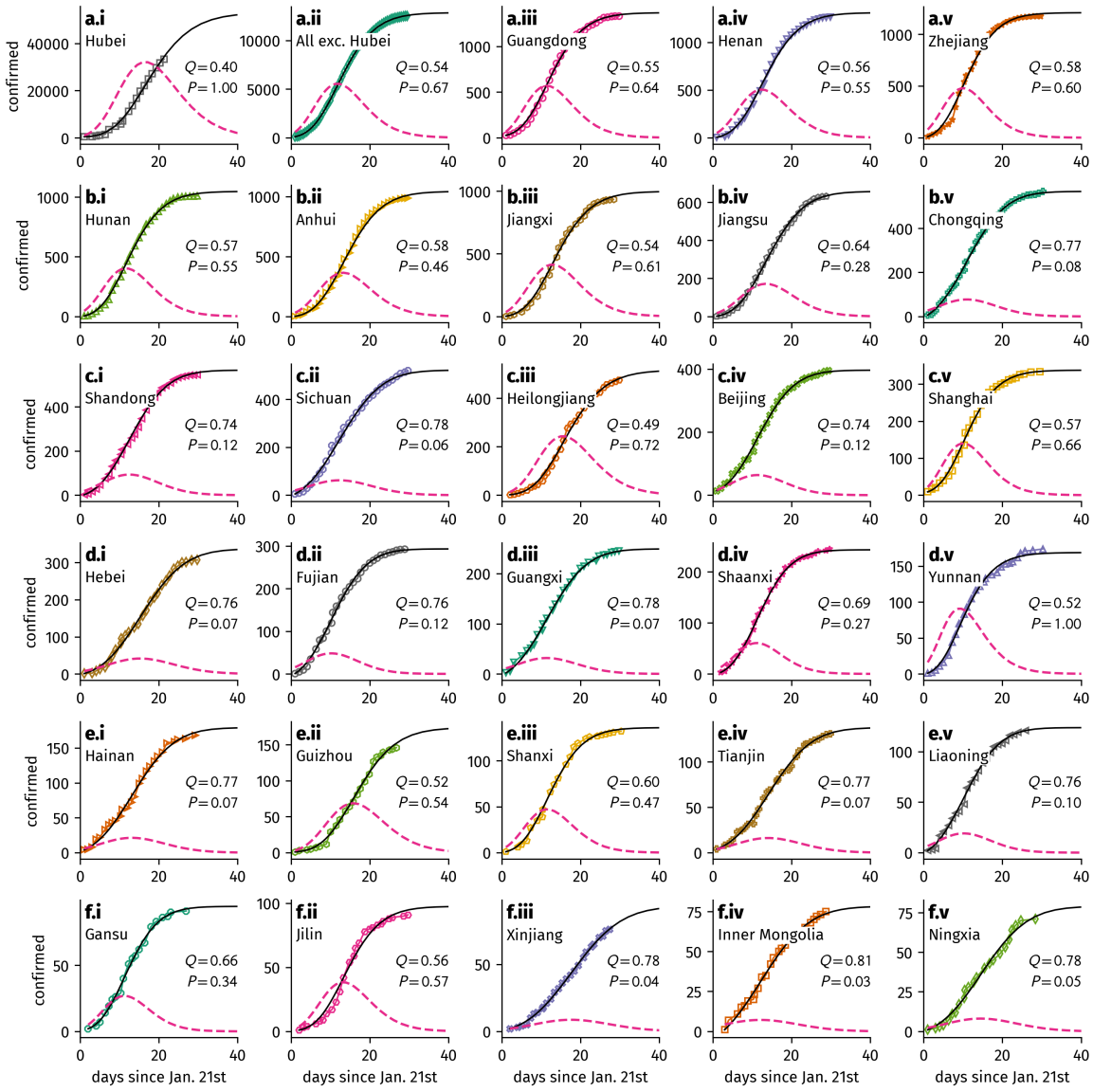

Figure S2: Case numbers of all affected provinces reproduced by the SIR-X model defined by Eqs. (1)-(4) of the main text and the fraction of unidentified infecteds $I(t)$ (dashed line) as obtained from least-squares fits.

Fig. S3.

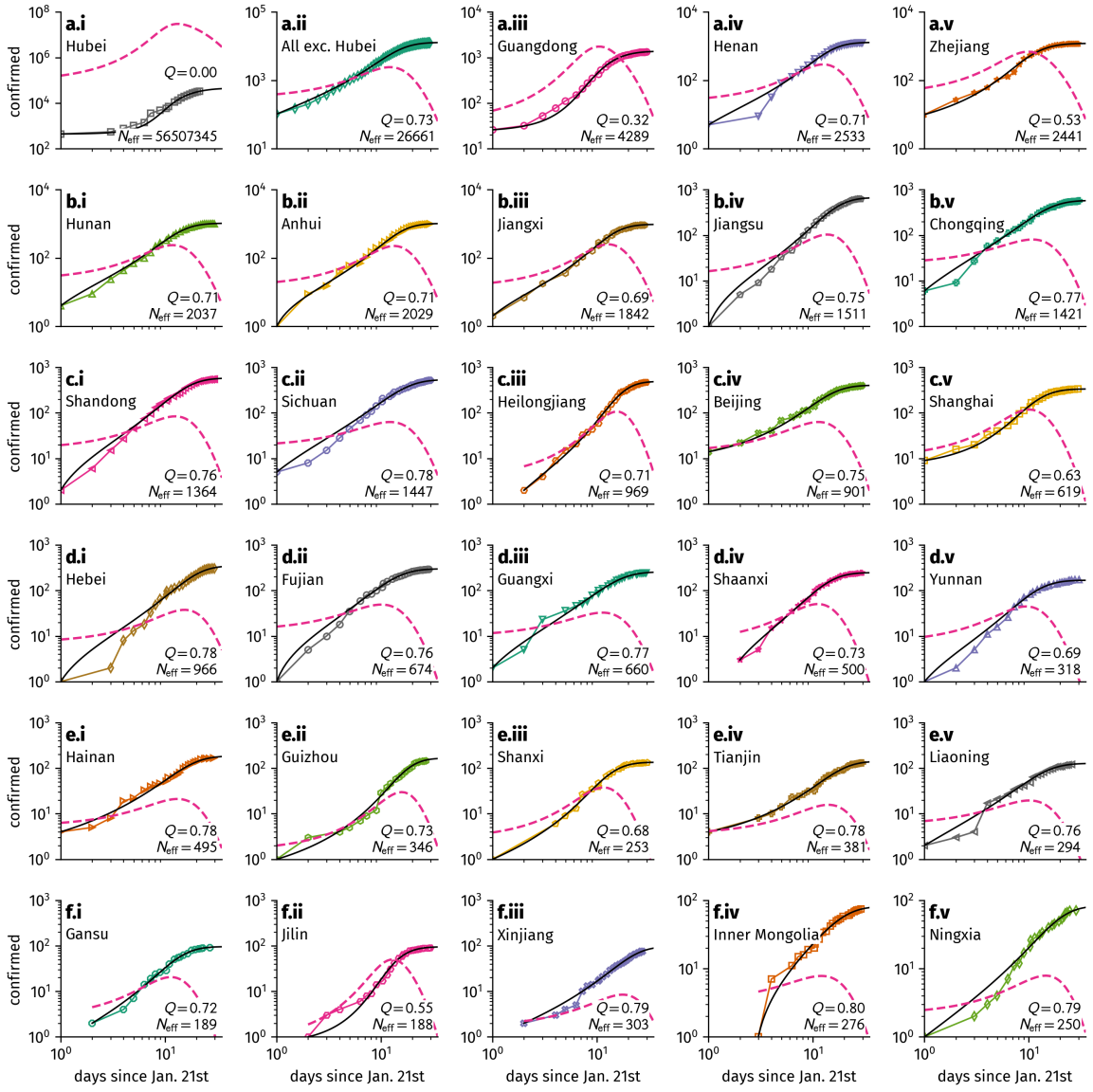

Figure S3: Case numbers of all affected provinces reproduced by the pure-quarantine model with fixed containment rate $\kappa_0 = 0$ and additional fit parameter effective population size $N_{\text{eff}} \ll N$, displayed on a log-log scale. Additionally shown is the fraction of unidentified infecteds $I(t)$ (dashed line) as obtained from least-squares fits. The restricted pure-quarantine model produces an unrealistically low value of quarantine probability for Hubei, suggesting that eventually, 56 million people will have been infected, virtually all of which would have gone unnoticed (see panel a.i).

Fig. S4.

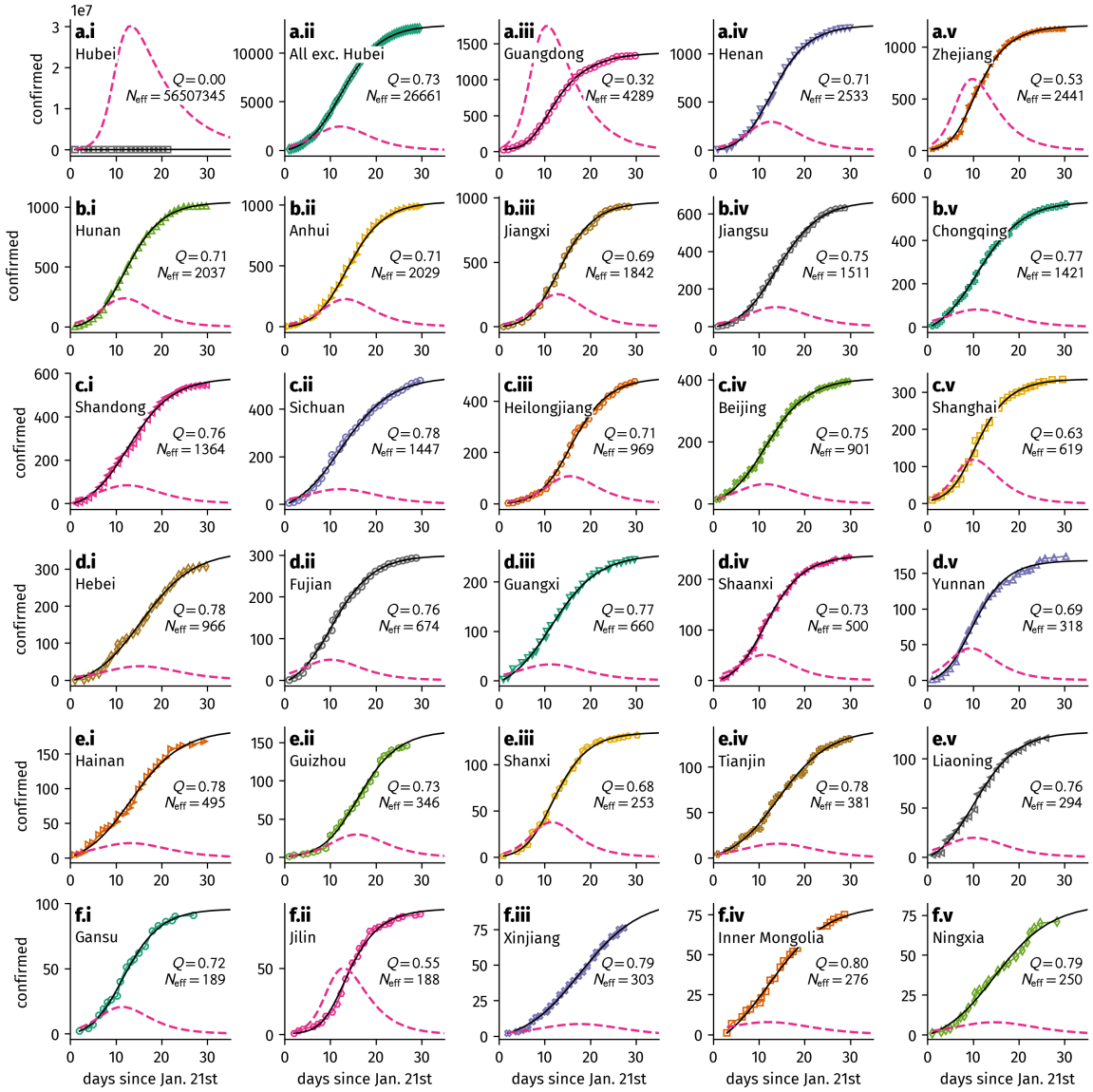

Figure S4: The results of the pure-quarantine model with fixed containment rate $\kappa_0 = 0$ and additional fit parameter effective population size $N_{\text{eff}} \ll N$ on a double-linear scale.

Fig. S5.

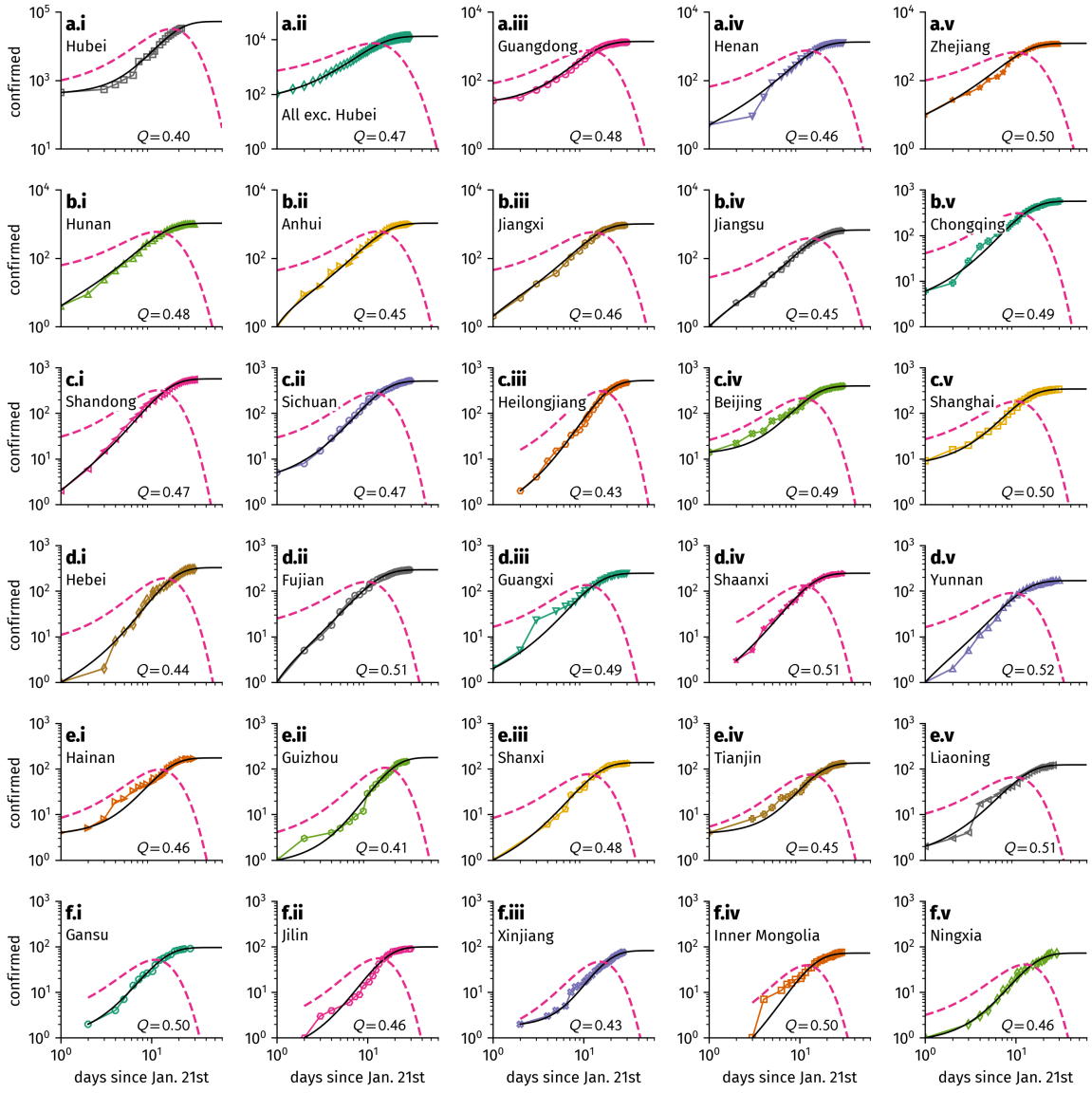

Figure S5: Case number fits for fixed quarantine rate $\kappa = 0$ where containment procedures affect the whole population (both infecteds and susceptibles) in a similar manner ($P = 1$). For Hubei, only data that was recorded before Feb. 13 was used, while for all other provinces model fits were performed for all available data points.

Fig. S6.

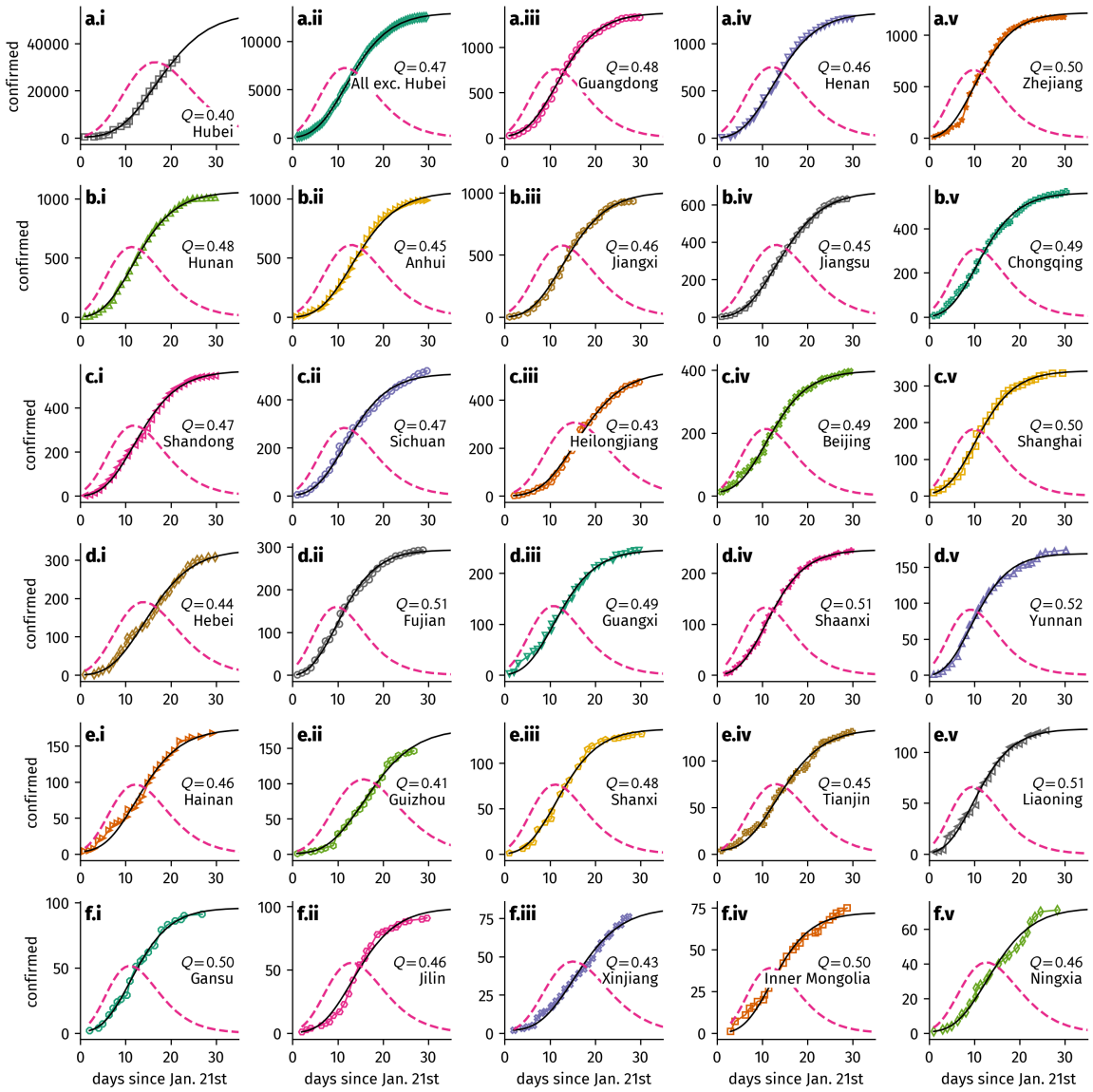

Figure S6: The results of the pure public-containment model with fixed quarantine rate $\kappa = 0$ on a double-linear scale.

Tab. S1.

Province	$N/10^6$	Q	P	κ [d^{-1}]	κ_0 [d^{-1}]	I_0/X_0	$R_{0,\mathrm{eff}}$
Hubei	57.1	0.47	0.66	0.038	0.073	2.55	3.28
All exc. Hubei	1277.8	0.69	0.21	0.219	0.058	6.98	1.93
Guangdong	104.3	0.51	0.75	0.032	0.099	3.66	3.02
Henan	94.3	0.61	0.38	0.122	0.074	41.00	2.41
Zhejiang	51.2	0.50	0.98	0.002	0.123	18.83	3.10
Hunan	67.0	0.47	1.00	0.000	0.111	58.34	3.28
Anhui	64.6	0.73	0.12	0.289	0.041	27.46	1.70
Jiangxi	44.0	0.44	1.00	0.000	0.099	19.41	3.46
Jiangsu	76.8	0.72	0.15	0.272	0.047	19.10	1.75
Chongqing	28.4	0.78	0.07	0.413	0.031	5.17	1.36

Table S1: Fit parameters used to model case number developments until Feb. 12th for Hubei and the remaining most affected provinces as displayed in Fig. 2, decreasingly ordered by largest case number. The quarantine probability reaches values of $Q = 0.6 \pm 0.1$ for these provinces while the public containment leverage P displays larger fluctuations. We further show the resulting effective basic reproduction number $R_{0,\mathrm{eff}}$ and fixed population size N as obtained from the *Geonames* project (*24*). Additionally, we report the obtained initial ratio of unidentified infectious to quarantined infecteds I_0/X_0.

Tab. S2.

Province	$N/10^6$	Q	P	$R_{0,\mathrm{eff}}$	κ [d^{-1}]	κ_0 [d^{-1}]	I_0/X_0
Hubei	57.1	0.40	1.00	3.71	0.000	0.084	2.26
All exc. Hubei	1277.8	0.54	0.67	2.86	0.049	0.097	5.67
Guangdong	104.3	0.55	0.64	2.79	0.055	0.099	2.55
Henan	94.3	0.56	0.55	2.71	0.073	0.088	9.84
Zhejiang	51.2	0.58	0.60	2.58	0.071	0.105	7.86
Hunan	67.0	0.57	0.55	2.65	0.075	0.092	11.73
Anhui	64.6	0.58	0.46	2.61	0.093	0.079	31.16
Jiangxi	44.0	0.54	0.61	2.86	0.057	0.089	17.69
Jiangsu	76.8	0.64	0.28	2.20	0.164	0.063	17.26
Chongqing	28.4	0.77	0.08	1.41	0.390	0.035	4.48
Shandong	94.2	0.74	0.12	1.63	0.309	0.042	9.66
Sichuan	87.2	0.78	0.06	1.37	0.413	0.028	4.05
Heilongjiang	38.2	0.49	0.72	3.18	0.033	0.086	6.61
Beijing	14.9	0.74	0.12	1.58	0.320	0.044	1.16
Shanghai	22.3	0.57	0.66	2.68	0.055	0.109	2.45
Fujian	36.9	0.76	0.12	1.52	0.341	0.045	15.60
Hebei	69.9	0.76	0.07	1.48	0.370	0.028	7.75
Guangxi	48.2	0.78	0.07	1.38	0.406	0.031	5.57
Shaanxi	37.6	0.69	0.27	1.94	0.201	0.073	4.35
Yunnan	45.4	0.52	1.00	2.99	0.000	0.134	16.13
Hainan	9.3	0.77	0.07	1.40	0.400	0.028	1.49
Guizhou	37.9	0.52	0.54	2.96	0.063	0.074	3.03
Shanxi	34.1	0.60	0.47	2.49	0.099	0.087	5.99
Liaoning	43.1	0.76	0.10	1.47	0.359	0.042	3.28
Tianjin	14.0	0.77	0.07	1.43	0.390	0.027	0.96
Gansu	26.3	0.66	0.34	2.13	0.157	0.082	2.53
Jilin	27.3	0.56	0.57	2.74	0.068	0.090	3.82
Xinjiang	21.3	0.78	0.04	1.34	0.435	0.019	1.01
Inner Mongolia	24.3	0.81	0.03	1.17	0.520	0.017	4.35
Ningxia	6.2	0.78	0.05	1.34	0.431	0.022	2.28

Table S2: Fit parameters for fits as described in the Materials and Methods with fixed population size N, and resulting effective basic reproduction number $R_{0,\mathrm{eff}}$ for all affected provinces, decreasingly ordered by largest case number. For Hubei, only data that was recorded before Feb. 13 was used, while for all other provinces model fits were performed for all available data points.

Tab. S3.

Province	Q	$R_{0,\mathrm{eff}}$	N_{eff}	κ [d^{-1}]	I_0/X_0
Hubei	0.00	6.00	56507345	0.000	364.02
All exc. Hubei	0.73	1.61	26662	0.340	3.81
Guangdong	0.32	4.06	4289	0.060	2.63
Henan	0.71	1.76	2534	0.302	6.16
Zhejiang	0.53	2.81	2442	0.141	5.98
Hunan	0.71	1.75	2037	0.303	7.73
Anhui	0.71	1.73	2029	0.308	19.87
Jiangxi	0.69	1.88	1842	0.275	9.46
Jiangsu	0.75	1.49	1511	0.378	16.25
Chongqing	0.77	1.39	1422	0.415	4.68
Shandong	0.76	1.44	1365	0.397	9.80
Sichuan	0.78	1.33	1448	0.440	4.27
Heilongjiang	0.71	1.74	969	0.306	3.36
Beijing	0.75	1.50	901	0.376	1.20
Shanghai	0.63	2.20	620	0.216	1.67
Fujian	0.76	1.47	675	0.387	16.13
Hebei	0.78	1.32	966	0.442	8.40
Guangxi	0.77	1.35	660	0.430	5.82
Shaanxi	0.73	1.64	501	0.333	4.11
Yunnan	0.69	1.84	319	0.283	9.62
Hainan	0.78	1.34	496	0.436	1.57
Guizhou	0.73	1.61	347	0.340	2.00
Shanxi	0.68	1.94	254	0.262	3.87
Liaoning	0.76	1.44	295	0.397	3.45
Tianjin	0.78	1.34	381	0.434	1.04
Gansu	0.72	1.69	190	0.318	2.24
Jilin	0.55	2.73	188	0.150	1.87
Xinjiang	0.79	1.26	303	0.469	1.11
Inner Mongolia	0.80	1.20	277	0.500	4.60
Ningxia	0.79	1.27	250	0.465	2.48

Table S3: Fit parameters for fixed public containment rate $\kappa_0 = 0$ where containment procedures are assumed to have had an immediate effect by reducing the population size N to an effective at-risk population size $N_{\mathrm{eff}} < N$ and the rise in confirmed cases is modeled by quarantine procedures only ($P = 0$). Again, we show the resulting effective basic reproduction number $R_{0,\mathrm{eff}}$. This restricted pure-quarantine model produces an unrealistically low value of quarantine probability for Hubei, suggesting that eventually, 56 million people will have been infected, virtually all of which would have gone unnoticed.

Tab. S4.

Province	$N/10^6$	Q	$R_{0,\mathrm{eff}}$	κ_0 [d^{-1}]	I_0/X_0
Hubei	57.1	0.40	3.71	0.084	2.26
All exc. Hubei	1277.8	0.47	3.28	0.111	6.96
Guangdong	104.3	0.48	3.23	0.115	3.18
Henan	94.3	0.46	3.33	0.108	13.15
Zhejiang	51.2	0.50	3.07	0.127	10.03
Hunan	67.0	0.48	3.25	0.113	15.56
Anhui	64.6	0.45	3.41	0.102	44.34
Jiangxi	44.0	0.46	3.38	0.105	22.63
Jiangsu	76.8	0.45	3.41	0.102	27.49
Chongqing	28.4	0.49	3.14	0.122	6.81
Shandong	94.2	0.47	3.29	0.110	15.29
Sichuan	87.2	0.47	3.26	0.113	5.85
Heilongjiang	38.2	0.43	3.54	0.094	7.87
Beijing	14.9	0.49	3.18	0.118	1.85
Shanghai	22.3	0.50	3.08	0.126	3.00
Fujian	36.9	0.51	3.06	0.129	25.02
Hebei	69.9	0.44	3.50	0.097	10.93
Guangxi	48.2	0.49	3.19	0.118	8.19
Shaanxi	37.6	0.51	3.06	0.128	6.86
Yunnan	45.4	0.52	2.99	0.134	16.13
Hainan	9.3	0.46	3.33	0.108	2.11
Guizhou	37.9	0.41	3.64	0.088	4.10
Shanxi	34.1	0.48	3.23	0.115	8.41
Liaoning	43.1	0.51	3.05	0.129	5.22
Tianjin	14.0	0.45	3.41	0.102	1.35
Gansu	26.3	0.50	3.09	0.126	3.81
Jilin	27.3	0.46	3.32	0.108	4.99
Xinjiang	21.3	0.43	3.51	0.096	1.30
Inner Mongolia	24.3	0.50	3.08	0.127	5.88
Ningxia	6.2	0.46	3.38	0.104	3.18

Table S4: Fit parameters for fixed quarantine rate $\kappa = 0$ and public containment rate $\kappa_0 > 0$, where it is assumed that all containment procedures affect the general population in the same way as infecteds ($P = 1$). We further show the resulting effective basic reproduction number $R_{0,\mathrm{eff}}$. Provinces are ordered decreasingly by largest case number.

Tab. S5.

Province	μ_{fit}	μ_{approx}	rel. err.
Hubei	2.32	2.39	0.03
All exc. Hubei	1.92	1.71	0.12
Guangdong	2.04	1.89	0.08
Henan	2.12	1.88	0.13
Zhejiang	2.16	1.72	0.25
Hunan	2.09	1.87	0.12
Anhui	2.05	1.73	0.19
Jiangxi	2.75	2.04	0.35
Jiangsu	2.20	1.67	0.32
Chongqing	1.45	1.36	0.07

Table S5: Comparison between scaling law exponents obtained from power-law fits and the analytical approximation derived in the Supplementary Text. Empirical exponents μ_{fit} correspond to the values shown in Fig. 1 of the main text. The approximate values μ_{approx} were computed on the basis of the SIR-X model parameters provided in table S1.

References and Notes

1. J. Cohen, Scientists are racing to model the next moves of a coronavirus that's still hard to predict. *Science* (2020). doi:10.1126/science.abb2161

2. WHO, Novel coronavirus (2019-nCoV) situation report - 11 (2020).

3. WHO, Coronavirus disease 2019 (COVID-19) situation report - 51 (2020).

4. CDC, 2019 Novel coronavirus (2019-nCoV), https://www.cdc.gov/coronavirus/2019-ncov/about/symptoms.html (accessed 13 February 2020).

5. J. Hsu, Here's how computer models simulate the future spread of new coronavirus. *Sci. Am.* (13 February 2020).

6. T. Lewis, China's citywide quarantines: Are they ethical and effective? *Sci. Am.* (25 January 2020).

7. N. Chen, M. Zhou, X. Dong, J. Qu, F. Gong, Y. Han, Y. Qiu, J. Wang, Y. Liu, Y. Wei, J. Xia, T. Yu, X. Zhang, L. Zhang, Epidemiological and clinical characteristics of 99 cases of 2019 novel coronavirus pneumonia in Wuhan, China: A descriptive study. *Lancet* **395**, 507–513 (2020). doi:10.1016/S0140-6736(20)30211-7

8. S. Zhao, Q. Lin, J. Ran, S. S. Musa, G. Yang, W. Wang, Y. Lou, D. Gao, L. Yang, D. He, M. H. Wang, Preliminary estimation of the basic reproduction number of novel coronavirus (2019-nCoV) in China, from 2019 to 2020: A data-driven analysis in the early phase of the outbreak. *Int. J. Infect. Dis.* **92**, 214–217 (2020). doi:10.1016/j.ijid.2020.01.050 Medline

9. E. Dong, H. Du, L. Gardner, An interactive web-based dashboard to track COVID-19 in real time. *Lancet* (2020). doi:10.1016/S1473-3099(20)30120-1

10. S. de Picoli Junior, J. J. Teixeira, H. V. Ribeiro, L. C. Malacarne, R. P. dos Santos, R. dos Santos Mendes, Spreading patterns of the influenza A (H1N1) pandemic. *PLOS ONE* **6**, e17823 (2011). doi:10.1371/journal.pone.0017823 Medline

11. A. G. Hunt, Exponential growth in Ebola outbreak since May 14, 2014. *Complexity* **20**, 8–11 (2014). doi:10.1002/cplx.21615

12. R. M. Anderson, R. M. May, *Infectious Diseases of Humans: Dynamics and Control*, Oxford Science Publications (Oxford Univ. Press, 1991).

13. Q. Li, X. Guan, P. Wu, X. Wang, L. Zhou, Y. Tong, R. Ren, K. S. M. Leung, E. H. Y. Lau, J. Y. Wong, X. Xing, N. Xiang, Y. Wu, C. Li, Q. Chen, D. Li, T. Liu, J. Zhao, M. Liu, W. Tu, C. Chen, L. Jin, R. Yang, Q. Wang, S. Zhou, R. Wang, H. Liu, Y. Luo, Y. Liu, G. Shao, H. Li, Z. Tao, Y. Yang, Z. Deng, B. Liu, Z. Ma, Y. Zhang, G. Shi, T. T. Y. Lam, J. T. Wu, G. F. Gao, B. J. Cowling, B. Yang, G. M. Leung, Z. Feng, Early Transmission Dynamics in Wuhan, China, of Novel Coronavirus-Infected Pneumonia. *N. Engl. J. Med.* **382**, 1199–1207 (2020). doi:10.1056/NEJMoa2001316 Medline

14. B. Prasse, M. A. Achterberg, L. Ma, P. Van Mieghem, Network-Based Prediction of the 2019-nCoV Epidemic Outbreak in the Chinese Province Hubei. arXiv:2002.04482 [physics, q-bio] (2020).

15. S. Sanche *et al*., The Novel Coronavirus, 2019-nCoV, is Highly Contagious and More Infectious Than Initially Estimated. arXiv:2002.03268 [q-bio] (2020).

16. Y. Chen, J. Cheng, Y. Jiang, K. Liu, A time delay dynamic system with external source for the local outbreak of 2019-nCoV. *Appl. Anal.* 1–12 (2020). doi:10.1080/00036811.2020.1732357

17. WHO, Report of the WHO-China joint mission on coronavirus disease 2019 (COVID-19) (2020).

18. M. J. Keeling, P. Rohani, *Modeling Infectious Diseases in Humans and Animals* (Princeton Univ. Press, 2008).

19. W. O. Kermack, A. G. McKendrick, Contributions to the mathematical theory of epidemics—I. 1927. *Bull. Math. Biol.* **53**, 33–55 (1991). Medline

20. WHO, Novel Coronavirus (2019-nCoV) Situation Report - 7 (2020).

21. A. J. Kucharski *et al.,* Early dynamics of transmission and control of COVID-19: A mathematical modelling study. *medRxiv* p. 2020.01.31.20019901 (2020). https://doi.org/10.1101/2020.01.31.20019901.

22. J. M. Read, J. R. Bridgen, D. A. Cummings, A. Ho, C. P. Jewell, Novel coronavirus 2019-nCoV: Early estimation of epidemiological parameters and epidemic predictions. *medRxiv* p. 2020.01.23.20018549 (2020). https://doi.org/10.1101/2020.01.23.20018549

23. B. F. Maier, https://github.com/CSSEGISandData/COVID-19 (accessed 29 March 2020). doi:10.5281/zenodo.3732556

24. GeoNames Project, GeoNames. https://geonames.org (accessed 1 November 2019).